catalysts

MDPI

*Article*

# Development of a γ-$Al_2O_3$-Based Heterogeneous Fenton-like Catalyst and Its Application in the Advanced Treatment of Maotai-Flavored Baijiu Wastewater

**Benfu Luo [1], Yujing Yan [1], Jinyin Li [2], Fei Guo [1,*], Weiwei Huang [2], Xi Yang [3], Haiyan Ning [1], Qicheng Kang [1], Haixing He [1], Xuanyu Zhou [1], Xiang Zhou [4], Shijie Wang [1] and Yuhang Liu [1]**

[1] School of Architecture and Civil Engineering, Xihua University, Chengdu 610039, China; kkllbbff@mail.xhu.edu.cn (B.L.); yooho666@outlook.com (Y.Y.)
[2] China Municipal Engineering Zhongnan Design and Research Institute Co., Ltd., Wuhan 430010, China
[3] Chengdu University Library, Chengdu 610106, China
[4] Suyi Design Group Co., Ltd., Nanjing 210012, China
* Correspondence: fei.guo@mail.xhu.edu.cn

**Abstract:** Heterogeneous Fenton technology was employed for the advanced treatment of Maotai-flavored Baijiu wastewater. Novel catalysts were prepared by loading different active ingredients (Mn, Fe, and Cu) on γ-$Al_2O_3$ using an impregnation method. The effects of active ingredient, reaction time, initial pH, $H_2O_2$ dosage, catalyst dosage, and other factors on the reaction were examined. The properties of the new catalysts were analyzed using BET analysis, XPS, and SEM. Moreover, the mechanisms of Fenton-like oxidation and its reaction kinetics were explored through experiments and analyses including GC–MS and intermediate active species scavenging by tertiary butyl alcohol (TBA) and/or para-benzoquinone. The results revealed that the most effective removal of organic matter was achieved with a Mn-Fe/Al (2:1 wt%) catalyst dosage of 30 g/100 g water, pH of 5.0, $H_2O_2$ dosage of 0.3 g/L, and reaction time of 60 min; the effluent COD value was 12 ± 1 mg/L, and the degradation rate was 65.7 ± 3%, approximately 14% higher than that of the conventional Fenton catalyst under similar conditions; moreover, the catalytic efficacy remained high after seven cycles. Kinetic analysis indicated that the heterogeneous Fenton oxidation reaction followed a third-order kinetics model, with $R^2$ = 0.9923 and K = 0.0006 $min^{-1}$.

**Keywords:** aluminum-based catalysts; heterogeneous Fenton; Maotai-flavored Baijiu wastewater; advanced oxidation processes; advanced treatment

check for updates

**Citation:** Luo, B.; Yan, Y.; Li, J.; Guo, F.; Huang, W.; Yang, X.; Ning, H.; Kang, Q.; He, H.; Zhou, X.; et al. Development of a γ-$Al_2O_3$-Based Heterogeneous Fenton-like Catalyst and Its Application in the Advanced Treatment of Maotai-Flavored Baijiu Wastewater. *Catalysts* **2024**, *14*, 422. https://doi.org/10.3390/catal14070422

Academic Editor: Enric Brillas

Received: 12 June 2024
Revised: 27 June 2024
Accepted: 28 June 2024
Published: 1 July 2024

**Copyright:** © 2024 by the authors. Licensee MDPI, Basel, Switzerland. This article is an open access article distributed under the terms and conditions of the Creative Commons Attribution (CC BY) license (https://creativecommons.org/licenses/by/4.0/).

## 1. Introduction

The production of Maotai-flavored Baijiu industrial wastewater in China increased annually from 2010 to 2022 [1]. Brewing wastewater is divided into high-concentration organic wastewater (distillation effluent and residual liquid) and low-concentration organic wastewater (cooling water, bottle-washing water, and site-rinsing water) [2,3]. The pollutant composition varies with the brewing stage. High-concentration organic wastewater is rich in organic matter such as starch, protein, amino acids, and sugars. It has a high chemical oxygen demand (COD), biochemical oxygen demand (BOD), suspended solids (SS) content, sulfur concentration, ammoniacal nitrogen (NH3-N) concentration, total nitrogen (TN) concentration, and total phosphorus (TP) concentration [4,5]. Maotai-flavored Baijiu wastewater is treated by anaerobic, biochemical, coagulation and oxidation methods, membrane filtration technology, and other combinations of enhanced processes. Water quality indicators other than COD can be reduced to the ideal level, while COD concentrations in the range of 30~80 mg/L necessitate further advanced treatment.

Advanced oxidation processes are characterized by an oxidizing capacity that surpasses that of common oxidants or an oxidation potential approaching that of hydroxyl

(·OH) radicals. ·OH radicals can initiate a series of free radical chain reactions with organic pollutants, destroying the structure of the pollutants and leading to their gradual degradation into harmless low-molecular-weight organics, ultimately converting them into $CO_2$, $H_2O$, and other mineral salts [6]. Advanced oxidation processes have become increasingly popular in recent years, with widespread application in laboratory pollutant degradation experiments and in practical engineering. This study presents a novel use of heterogeneous Fenton-like technology to degrade real wastewater with experimental investigations of heterogeneous Fenton-like oxidation under complex conditions.

Conventional Fenton technology uses $H_2O_2$ to generate ·OH under the catalytic effect of $Fe^{2+}$ to oxidize organic pollutants and treat wastewater [7,8]. During the conventional Fenton reaction, the pH is adjusted to 2−3, and the reaction conditions are harsh. Before the effluent can be discharged, the pH needs to be adjusted to neutral after the completion of the reaction. Additionally, conventional Fenton technology generates a large amount of iron sludge, which needs to be treated and disposed of. The catalyst cannot be recycled, and thus, the disposal costs are high. These issues significantly limit the practical application of conventional Fenton technology, which has led to the emergence of heterogeneous Fenton technology.

The heterogeneous Fenton process, in which $Fe^{2+}$ or active components are loaded onto a functional carrier, enables the Fenton reaction or the Fenton-like reaction to proceed in the solid–liquid state to degrade pollutants. The goal of this technique is to enhance treatment effectiveness while addressing the challenges in the traditional Fenton process, including the complexity of catalyst recovery, potential secondary contamination from catalyst deactivation by iron ions, and the need for a low pH [7]. Furthermore, in contrast to heterogeneous Fenton techniques, heterogeneous Fenton offers a broader pH range and greater $H_2O_2$ utilization and enables easy separation and recycling of the heterogeneous catalyst [9]. Moreover, the concentration of active ingredients dissolved in the catalyst can be controlled to promote their stability and efficient utilization and therefore limit the production of iron sludge.

In recent years, advanced treatment of wastewater has been the focus of several studies. These include the use of polyaluminum silicate sulfate (PASS) [10], Fenton-like reactions (modified ceramsite [11], Fe/Ce-RGO [12], and $Fe^0$ [13]), and Wang's preparation of novel PASS coagulant for effective advanced treatment of coking wastewater. The parameters used were a dosage of 7 mmol/L PASS, flocculation time of 30 min and pH of 7, which reduced the COD in cooking wastewater from 196.67 mg/L to 59.94 mg/L [10]. Wan utilized Fenton and heterogeneous Fenton-like technologies for advanced treatment of municipal secondary wastewater, with the SCOD degradation efficiency of the Fe/CeRGO heterogeneous Fenton-like reaction reaching 63.10% [12]. These novel advanced treatment methods are more economically feasible and simpler, and the heterogeneous Fenton technology is a particular focus of research compared to advanced treatment methods.

Various studies have verified the effectiveness of diverse substances as heterogeneous Fenton-like catalysts, including $Fe_3O_4$ [14], $Fe_3O_4$/MWCNTs [15], $CoFe_2O_4$ [16], $CuFe_2O_4$ [17], $NiFe_2O_4$ [18], $MnFe_2O_4$ [19], and Fe/$\gamma$-$Al_2O_3$ [20–22]. P. Bautista et al. employed the impregnation method to synthesize a custom Fe/$\gamma$-$Al_2O_3$ catalyst and studied its degradation impact on cosmetic wastewater. This Fe/$\gamma$-$Al_2O_3$ catalyst effectively degraded cosmetic wastewater with a COD concentration of 4560 mg/L using a catalyst dosage of 5 g/L and $H_2O_2$ dosage of 9050 mg/L, achieving an 85% degradation rate in 4 h [20]. The study concluded that this material can efficiently catalyze the heterogeneous Fenton-like reaction and is effective at degrading organic pollutants. In this study, $\gamma$-$Al_2O_3$ was chosen as the catalyst carrier to ensure catalyst stability and activity and in consideration of economic and practical aspects.

Aluminum oxide ($Al_2O_3$) has eight forms. $\gamma$-$Al_2O_3$ is one of the many forms of alumina that serve as a suitable carrier material for heterogeneous Fenton-like catalysts, exhibiting excellent physicochemical stability, a high specific surface area and porosity [23], and good potential for application.

In the present study, pretreated γ-$Al_2O_3$ was utilized as the catalyst carrier, and Mn, Fe, and Cu were loaded onto the carrier as active components using the impregnation method. The aims of this study were to assess the effectiveness of the catalyst in the advanced treatment of Maotai-flavored Baijiu wastewater, analyze its characteristics and performance, establish the optimal reaction conditions and kinetics, investigate the reaction mechanism, and explore the potential of heterogeneous Fenton-like technology for practical applications.

## 2. Results and Discussion

### *2.1. Catalyst Characterisation*

BET, XPS, and SEM analyses were performed on two catalysts: Mn-Fe (2:1 wt%)–γ-$Al_2O_3$ and Mn-Fe (2:2 wt%)–γ-$Al_2O_3$.

The changes in the specific surface area, pore volume, and pore diameter of γ-$Al_2O_3$ before and after high-temperature calcination and loading of the active ingredient were assessed. The BET results in Table 1 indicate that these parameters increased after high-temperature calcination but decreased after loading of the active ingredient.

**Table 1.** Analysis of catalyst pores and other structures.

| Catalyst Performance | BET Specific Surface Area ($m^2$/g) | Pore Volume ($cm^3$/g) | Average Pore Diameter (nm) |
|---|---|---|---|
| γ-$Al_2O_3$ | 201.50 | 0.40 | 8.30 |
| γ-$Al_2O_3$ (600 °C, 4 h) | 236.10 | 0.68 | 12.80 |
| Mn-Fe/Al (Mn:Fe = 2:1) | 151.50 | 0.45 | 11.84 |
| Mn-Fe/Al (Mn:Fe = 2:2) | 151.70 | 0.43 | 11.46 |

The SEM analysis in Figure 1 revealed that the surface of γ-$Al_2O_3$ after calcination exhibited more folding and had a larger surface area. However, after the loading process, the active ingredient filled the surface depressions, leading to a reduction in surface area. Additionally, the active ingredient occupied some of the pore space.

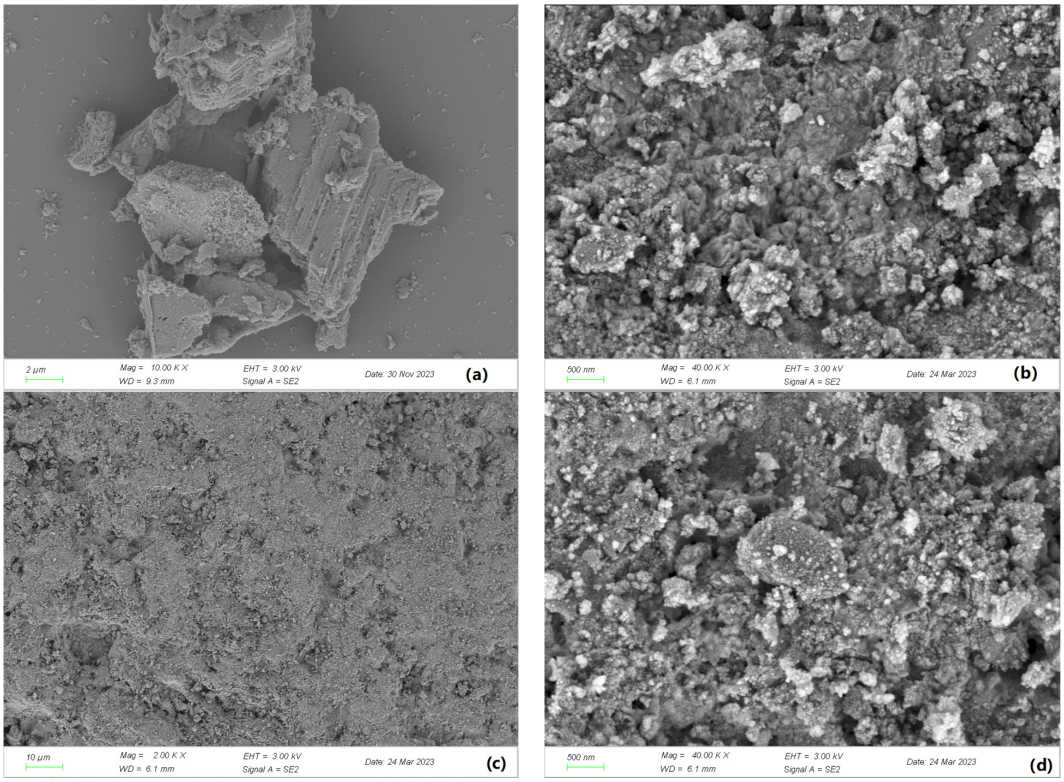



**Figure 1.** *Cont.*

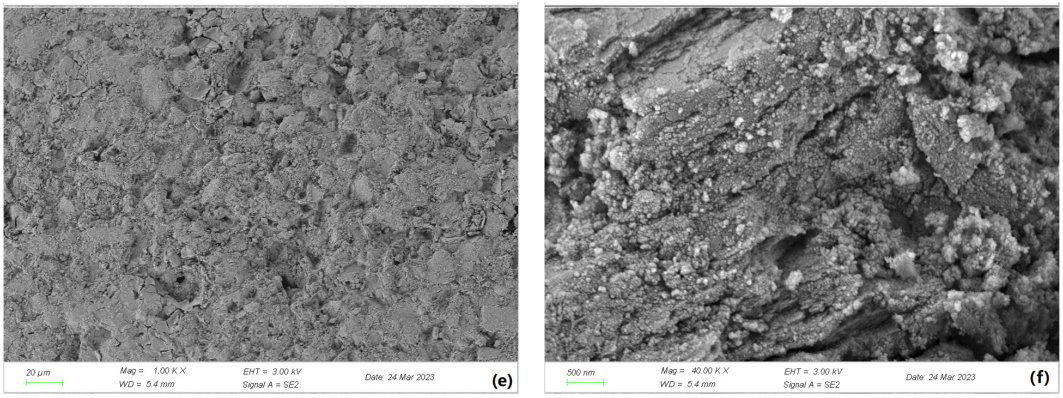



**Figure 1.** SEM images of γ-$Al_2O_3$ composite catalysts: (**a**) γ-$Al_2O_3$ (before calcination); (**b**) γ-$Al_2O_3$ (after calcination); (**c**) Mn-Fe (wt%2:wt%1)-γ-$Al_2O_3$ (10 µm); (**d**) Mn-Fe (wt%2:wt%1)-γ-$Al_2O_3$ (500 nm); (**e**) Mn-Fe (wt%2:wt%2)-γ-$Al_2O_3$ (20 µm); (**f**) Mn-Fe (wt%2:wt%2)-γ-$Al_2O_3$ (500 nm).

By comparing two different catalysts, it was observed that a small amount of Fe from the active ingredient was loaded onto the non-concave surface. As the Fe content in the active ingredient increased, the catalyst area slightly increased.

These findings suggest that the properties of the catalyst, such as surface area and pore characteristics, are influenced by both the calcination process and the loading of the active ingredient.

The XPS full spectra of the two catalysts, as depicted in Figure 2, displayed characteristic peaks corresponding to Al(2p) and O(1s) in γ-$Al_2O_3$ at 74.05 eV and 528.48 eV, respectively. The active components Fe(2p) and Mn(2p) exhibited characteristic peaks at 712.82 eV and 640.84 eV [24,25], respectively, while the characteristic peak of C(1s) was observed at 285.47 eV.

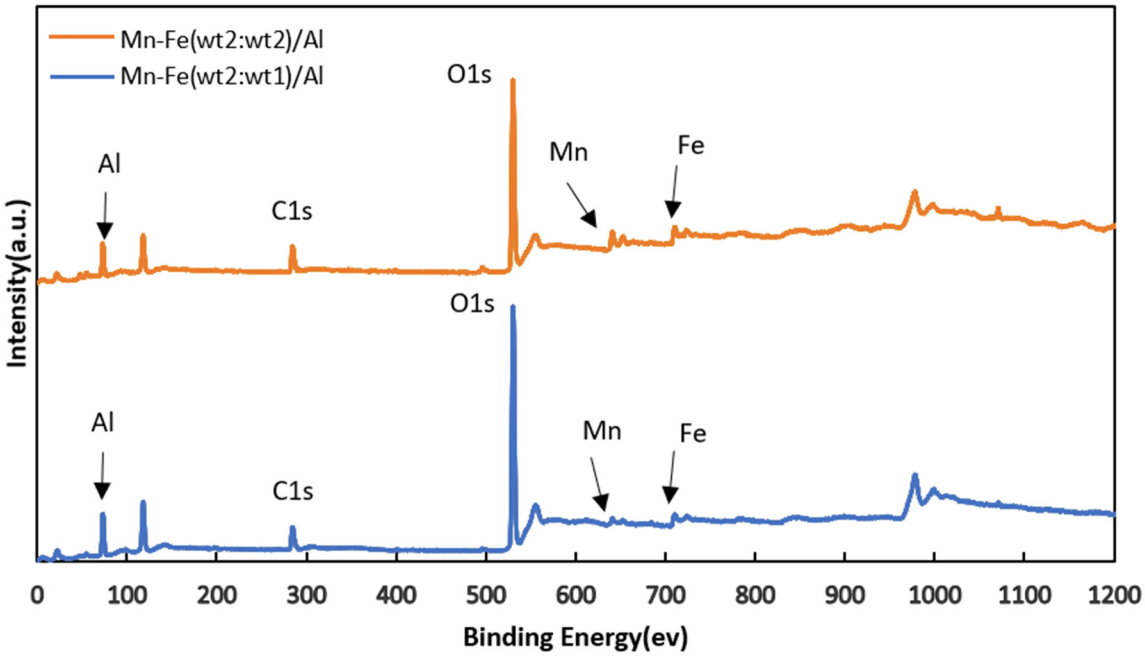



**Figure 2.** XPS spectra of Mn-Fe (wt%2:wt%1)/Al and Mn-Fe (wt2:wt2)/Al catalysts.

Upon comparing the full XPS spectra of the two catalysts, it was noted that there were no significant changes in elemental valence states. This indicates that there were no changes in the types of active components in the prepared catalysts, even when the amount of precursor solution was varied while keeping the precursor composition constant.

Subsequently, XRD detection was performed on Mn-Fe/$\gamma$-$Al_2O_3$. According to the XRD results in Figure 3, the composition of the catalyst is consistent with our speculation.

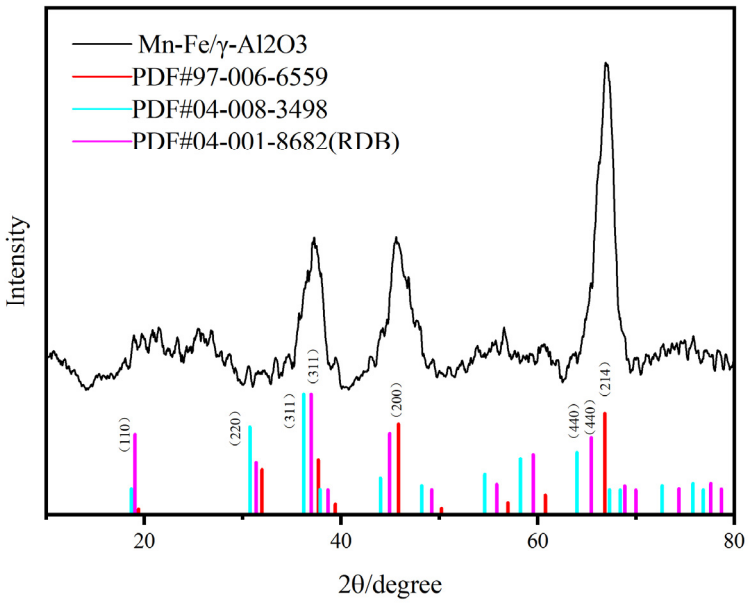



**Figure 3.** XRD images of Mn-Fe /$\gamma$-$Al_2O_3$ catalyst.

The SEM images in Figure 3 illustrate significant changes in the morphology of $\gamma$-$Al_2O_3$ before and after calcination. In Figure 1a, the surface of $\gamma$-$Al_2O_3$ appears smooth with no evident loading, while Figure 1b shows an uneven granular morphology with particles of different sizes and both concave and convex regions. The numerous irregular pores between these particles enhance the contact area for loading active ingredients. The loading capacity was notably affected by the presence of ash on the carrier surface, which hindered active ingredient loading and caused the collapse of some pores; these effects can be mitigated through calcination to aid active ingredient loading.

Figure 1d,f show that the depressions of $\gamma$-$Al_2O_3$ were filled, indicating the successful loading of active ingredients onto the surface. In contrast, Figure 1c,e show active ingredients filling the depressions with a uniform distribution on the catalyst surface. The protrusions in Figure 1e resulted from the loading of a small amount of Fe into nonconcave areas on the catalyst surface when the Fe active ingredient content was increased. We speculate that the protruding active component Fe on the surface may suffer from leaching during the reaction process due to its prominent state, as observed in the experimental catalytic effect of different catalyst types. It is evident that even though it exhibits good catalytic performance in the initial stages of the reaction, its later performance is inferior to that of the Mn-Fe/$\gamma$-$Al_2O_3$ (2:1 wt%) catalyst. Based on this, we infer that its stability is also not as good as that of the Mn-Fe/$\gamma$-$Al_2O_3$ (2:1 wt%) catalyst.

### *2.2. Effect of Catalyst Type on the Removal of COD from Maotai-Flavored Baijiu Wastewater*

To investigate the effects of different kinds and ratios of active ingredients loaded onto $\gamma$-$Al_2O_3$ as catalysts for the heterogeneous Fenton-like reaction on COD removal, 100 g of catalyst was added to 200 mL water samples, and 30% hydrogen peroxide was added at a concentration of 0.1 g/L. The reaction pH was adjusted to 5 to investigate the effects of different catalysts on the removal of COD from Maotai-flavored Baijiu wastewater.

As depicted in Figure 4, the catalysts prepared by loading various active ingredients onto $\gamma$-$Al_2O_3$ exhibited significantly different effects on the heterogeneous Fenton-like treatment of COD in Maotai-flavored Baijiu wastewater. Fourteen catalysts were prepared, including Mn-Fe, Mn-Cu, and Mn-Fe-Cu, with different weight ratios [26–29]. Among the catalysts, the Mn-Cu catalysts resulted in higher posttreatment COD levels exceed-

ing 23 ± 1 mg/L. Conversely, the Mn-Fe and Mn-Fe-Cu catalysts demonstrated greater effectiveness, with effluent COD levels generally below 16 mg/L. Specifically, the Mn-Fe catalysts with weight ratios of 2:1 wt% and 2:2 wt% exhibited even lower COD levels at 13 ± 1 mg/L. Considering factors such as cost effectiveness and catalyst stability [30–32], the Mn-Fe catalyst with a weight ratio of 2:1 wt% was selected for further experiments based on its COD-removal performance.

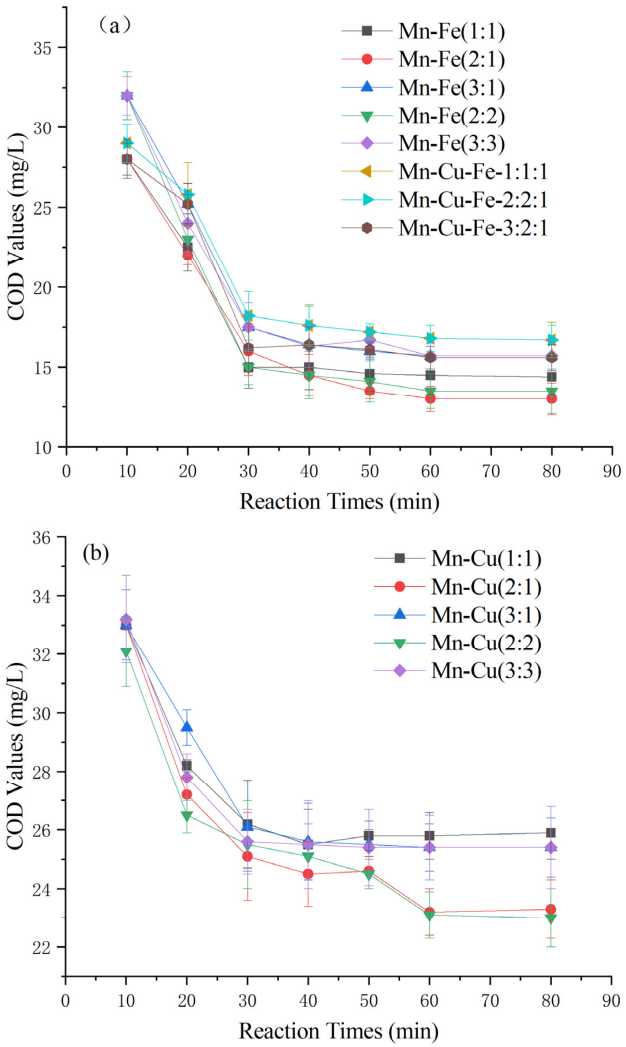



**Figure 4.** Effect of catalyst types on COD of Maotai-flavored Baijiu wastewater treated by heterogeneous Fenton-like reaction: (**a**) Mn-Fe type and Mn-Fe-Cu type; (**b**) Mn-Cu type.

### *2.3. Effect of Reaction Time on the Removal of COD from Maotai-Flavored Baijiu Wastewater*

To investigate the impact of varying reaction times on the treatment efficiency of the heterogeneous Fenton-like reaction, different reaction durations (10 min, 20 min, 30 min, 40 min, 50 min, 60 min, and 80 min) were studied. The experiment involved the addition of 100 g of Mn-Fe (2:1 wt%) catalyst, a 30% hydrogen peroxide dose of 0.1 g/L, and a reaction pH of 5. The experiment aimed to assess the effect of the heterogeneous Fenton-like reaction on the removal of COD from Maotai-flavored Baijiu wastewater at different time intervals.

Figure 5 shows that the initial 30 min of the reaction was highly effective, with a noticeable reduction in COD over time. Beyond 30 min, the rate of COD reduction started to slow, and by 60 min, it began to stabilize. Notably, at the 60 min mark, the COD-removal rate peaked at 66 ± 3%, with the COD value stabilizing at 12 ± 1 mg/L.

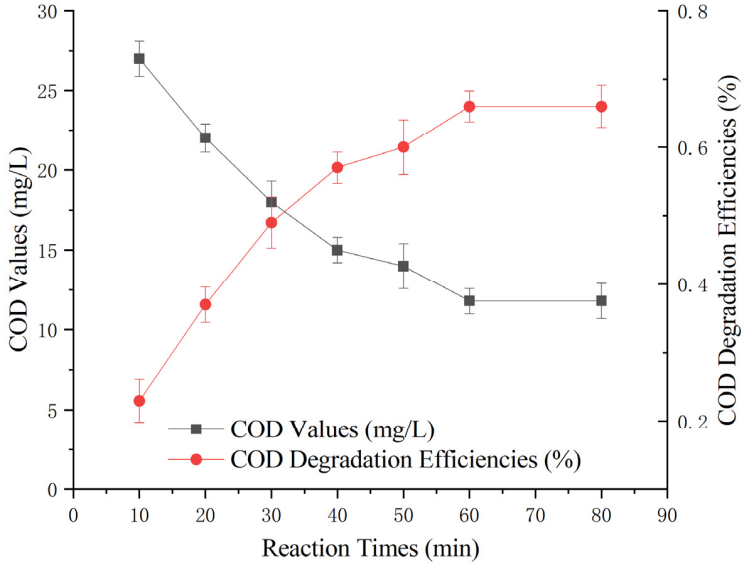



**Figure 5.** Effect of time on heterogeneous Fenton-like treatment of Maotai-flavored Baijiu wastewater.

The data suggest that prolonging the treatment time does not necessarily lead to a substantial improvement in treatment efficacy. Therefore, based on this analysis, the optimal heterogeneous Fenton-like treatment time was determined to be 60 min.

### *2.4. Effect of Initial pH on the Removal of COD from Maotai-Flavored Baijiu Wastewater*

To explore whether this heterogeneous Fenton-like process requires similarly stringent pH conditions as conventional Fenton reactions [6], the initial pH levels for this experiment were set at 3.5, 4.0, 4.5, 5.0, 5.5, and 6.0. The experiment involved the addition of 100 g of Mn-Fe (2:1 wt%) catalyst and a 30% hydrogen peroxide dose of 0.1 g/L, and the aim was to determine the optimal reaction pH.

Figure 6 shows that as the pH changed from acidic to neutral, the ability of the heterogeneous Fenton-like process to remove COD from Maotai-flavored Baijiu wastewater initially increased and then decreased. The greatest COD removal was observed at an initial pH of 5.0. This suggests that a relatively neutral pH is more suitable for this reaction than for conventional Fenton reactions, reducing the need for strongly acidic conditions.

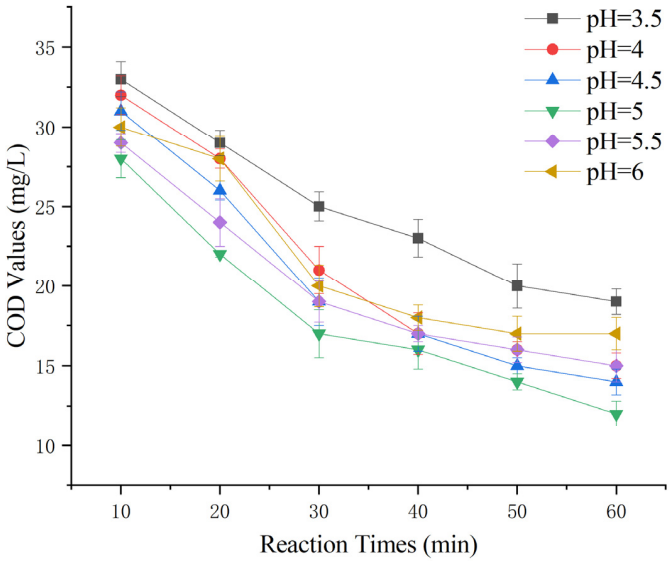



**Figure 6.** Effect of initial pH on heterogeneous Fenton-like treatment of Maotai-flavored Baijiu wastewater.

### *2.5. Effect of $H_2O_2$ Dosage on the Removal of COD from Maotai-Flavored Baijiu Wastewater*

To investigate the impact of varying initial $H_2O_2$ dosages on the removal of COD from Maotai-flavored Baijiu wastewater using heterogeneous Fenton-like reactions, an experiment was conducted under the following conditions: 100 g of Mn-Fe (2:1 wt%) catalyst, a reaction time of 60 min, and a reaction pH of 5. $H_2O_2$ (3%) was prepared by diluting 30% $H_2O_2$ tenfold, and dosages of 0.1 g/L, 0.2 g/L, 0.3 g/L, 0.4 g/L, 0.5 g/L, and 0.6 g/L were applied [23].

Observing from Figure 7, the COD-removal performance of Maotai-flavored Baijiu wastewater increased and then decreased with increasing $H_2O_2$ dosage. The treatment efficacy was strongest when the 3% $H_2O_2$ dosage was 0.3 g/L and decreased when the dosage exceeded or fell below this level. The analysis indicated that, similar to classical Fenton reactions, ·OH played a crucial role in determining the treatment efficacy. Lower $H_2O_2$ dosages resulted in insufficient ·OH, leading to inadequate oxidative strength, while higher dosages generated excessive ·OH, triggering a quenching reaction: Excessive ·OH converts $Fe^{2+}$ to $Fe^{3+}$, and ·OH further reacts with itself to produce $H_2O_2$ [33,34]. It is speculated that an excess of hydroxyl radicals could also lead to the conversion of $Mn^{2+}$ to $Mn^{3+}$. All of these can result in the ineffective decomposition of $H_2O_2$, which reduced the efficiency of the $H_2O_2$ reaction.

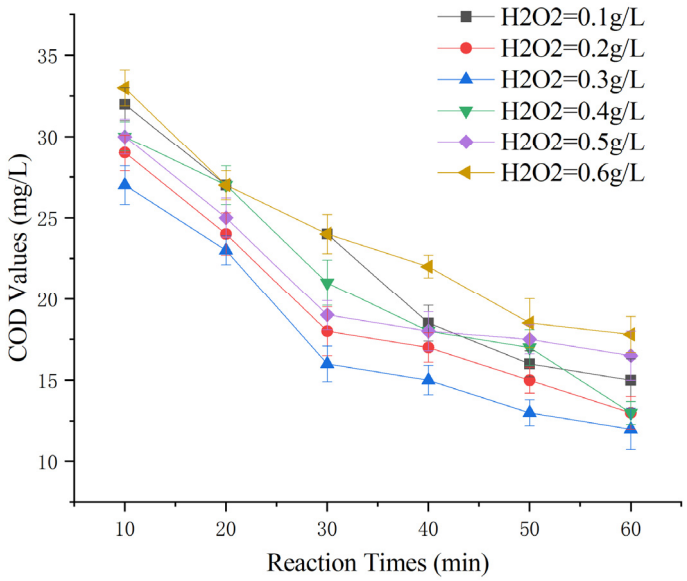



**Figure 7.** Effect of $H_2O_2$ dosage on heterogeneous Fenton-like treatment of Maotai-flavored Baijiu wastewater.

### *2.6. Effect of Catalyst Dosage on the Removal of COD from Maotai-Flavored Baijiu Wastewater*

To determine the optimal catalyst dosage for the reaction, experiments were conducted under consistent conditions: a 3% hydrogen peroxide dose of 0.3 g/L, a pH of 5, a reaction time of 60 min, and varying amounts of Mn-Fe (2:1 wt%) catalyst (4 g, 10 g, 20 g, 60 g, 100 g, 140 g, and 180 g). The impact of these different catalyst dosages on the removal of COD from Maotai-flavored Baijiu wastewater through heterogeneous Fenton-like oxidation was examined.

Figure 8 shows that as the catalyst dosage increased, the effectiveness of the heterogeneous Fenton-like treatment continuously improved. The treatment efficacy peaked at a catalyst dosage of 60 g, with a reduction in effluent COD to 12 ± 1 mg/L and a removal rate of 64%. At catalyst dosages above 60 g, the treatment efficacy did not increase further; rather, it started to decrease, with the decline becoming more pronounced at dosages exceeding 100 g.

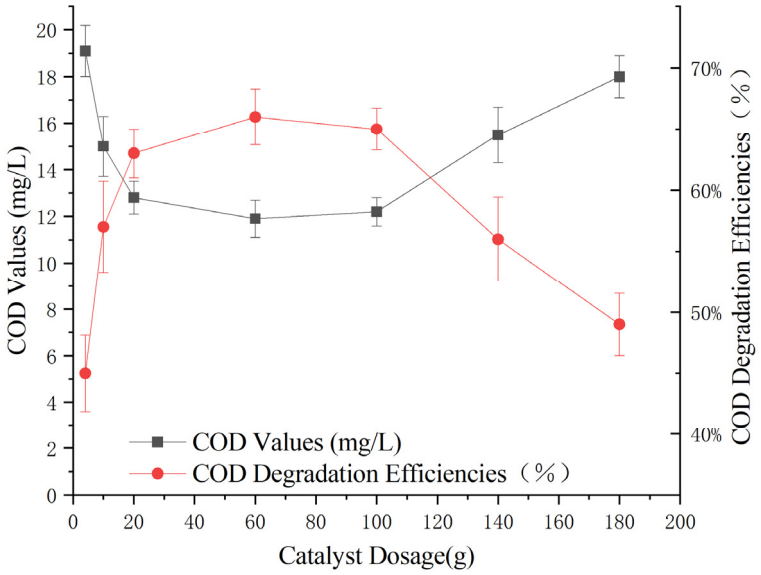



**Figure 8.** Effect of catalyst dosage on heterogeneous Fenton-like treatment of Maotai-flavored Baijiu wastewater.

The above results indicate that the optimal catalyst dose for this reaction is approximately 60 g, where the treatment effect is maximized. Increasing the catalyst dosage beyond this point does not yield additional benefits and may even lead to a reduction in treatment efficiency.

Based on the data and reasoning provided, along with insights from the reaction mechanism (see Section 2.8 for details) [35,36], it is evident that when the catalyst dose exceeded 60 g, the treatment effect did not improve but rather decreased. This decline in treatment efficacy can be attributed to catalyst overdosage, which led to certain detrimental effects on the reaction process.

First, an excessive amount of dissolved active ingredients such as $Fe^{2+}$ and $Mn^{2+}$ in the water resulted in the accelerated cycling of $Fe^{2+}/Fe^{3+}$ species. This accelerated cycling led to the rapid and extensive consumption of $H_2O_2$, causing a significant increase in the production of free hydroxyl radicals (·OH) with a very short half-life (on the order of $10^{-9}$ s). These highly reactive ·OH radicals, in turn, reacted with each other to regenerate $H_2O_2$ rather than effectively degrading the pollutants in the water samples. This process hindered oxidation and reduced the treatment efficiency.

Second, the nonselective nature of hydroxyl radical oxidation reactions resulted in the formation of undesirable byproducts when ·OH reacted with active components in water. These byproducts interfered with the oxidative degradation of pollutants, further diminishing the overall effectiveness of the reaction mechanism.

Therefore, maintaining the catalyst dosage within an optimal range, such as the experimentally observed value of approximately 60 g, is crucial to ensure efficient pollutant degradation and prevent the negative impacts associated with catalyst overdosage.

### *2.7. Catalyst Stability Analysis*

To assess the stability of the Mn-Fe catalyst under optimal parameters, a continuous reaction experiment was conducted using 60 g of catalyst, a 3% hydrogen peroxide dose of 0.3 g/L, a reaction pH of 5, and continuous aeration at the bottom of the reactor. The initial COD of the wastewater was measured to be 35 ± 1 mg/L.

After 60 min, the supernatant was collected, centrifuged, and filtered for COD measurement using the potassium dichromate method. After sampling, all the water was removed by filtration, the original catalyst was retained, and a new round of wastewater was reintroduced to continue the reaction.

By monitoring the effectiveness of the catalyst in removing COD from Maotai-flavored Baijiu wastewater over multiple reaction cycles, this study aimed to evaluate the catalyst's stability and ability to maintain consistent pollutant degradation performance over time.

According to Figure 9, the treatment effect of the heterogeneous Fenton-like reaction gradually decreased with increasing number of cycles. However, the effluent COD remained at approximately 12 ± 1 mg/L within eight cycles. The results indicate that the catalyst exhibited good stability, supporting its potential application in the advanced treatment of Maotai-flavored Baijiu wastewater.

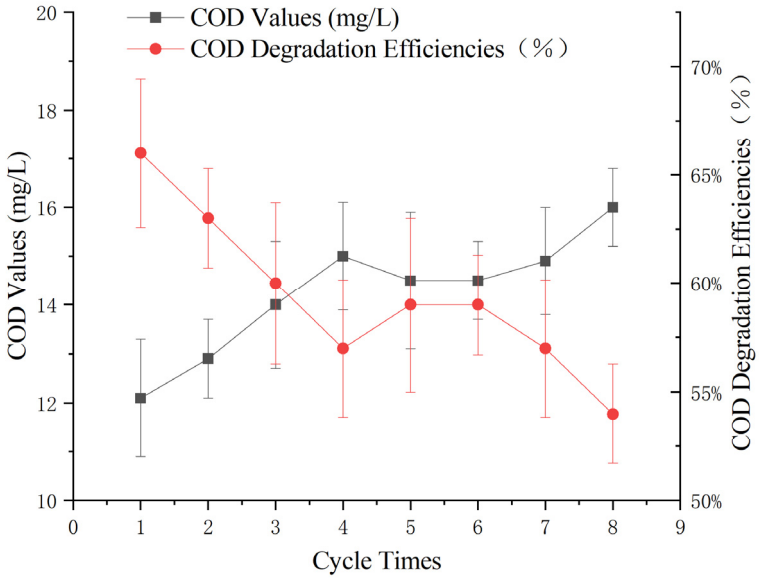



**Figure 9.** Effect of the number of wastewater cycles on heterogeneous Fenton-like treatment of Maotai-flavored Baijiu wastewater.

A comparison of this type of Fenton reaction with the research of other scholars is presented in Table 2.

**Table 2.** Compare the results with the reported values in the literature.

| Catalysts and Reagents | Wastewater Type | Results |
|---|---|---|
| $CuFe_2O_4$ + TA + $H_2O_2$ [37] | Methylene blue | The results showed that introducing TA enhanced MB decolorization rate from 52.0% to 92.1% within 80 min [37]. |
| $MnFe_2O_4$/biochar + $H_2O_2$ [19] | Methylene blue | When using the $MnFe_2O_4$/BC composite as an ultrasound-assisted heterogeneous Fenton-like catalyst, 95% of MB (20 mg/L) was degraded at pH = 5 in the presence of 15 mmol/L $H_2O_2$ in 20 min [19]. |
| Polyaluminum silicate sulfate [10] | Coking wastewater | A dosage of 7 mmol/L PASS, flocculation velocity of 75 r/min, flocculation time of 30 min, pH of 7, and temperature of 20 °C could decrease the COD concentration from 196.67 mg/L to 59.94 mg/L [10]. |
| Fe/Ce-RGO + $H_2O_2$ [12] | Municipal secondary effluent | The removal efficiencies of DOC, SCOD, and SMT were 36.30%, 63.10%, and 35.00% using Fe/CeRGO as catalyst [12]. |

**Table 2.** *Cont.*

| Catalysts and Reagents | Wastewater Type | Results |
| --- | --- | --- |
| Fe0 + $H_2O_2$ [13] | Citric acid wastewater | When the initial pH was 3.0, $H_2O_2$/COD = 0.7 × $Fe_0/H_2O_2$ = 3.29 (weight ratio), coagulation pH = 9.0, and the COD removal reached to over 35% in 2 h [13]. |
| Modified ceramsite + $H_2O_2$ + MBFB (Fenton-like/MBFB) [11] | Synthetic dye wastewater | The optimal conditions were $H_2O_2$ concentration of 600 mg/L and HRT of 6 h, while the influent COD concentration was 90 mg/L, achieving COD-removal efficiency of 64.8%. |
| Mn-Fe/γ-$Al_2O_3$ + $H_2O_2$ | Maotai-flavored Baijiu wastewater | The results revealed that the most effective removal of organic matter was achieved with a Mn-Fe/γ-$Al_2O_3$ catalyst dosage of 30 g/100 g water, pH of 5.0, $H_2O_2$ dosage of 0.3 g/L, and reaction time of 60 min, while the influent COD concentration is 35 mg/L; the effluent COD value was 12 ± 1 mg/L, and the degradation rate was 65.7 ± 3%. |

### *2.8. Reaction Kinetics Studies*

According to the above analyses, the best treatment effect of this heterogeneous Fenton-like reaction was obtained when the Mn-Fe/γ-$Al_2O_3$ (2:1 wt%) catalyst was used at pH 5.0, a catalyst dosage of 30 g (100 g water), a 3% $H_2O_2$ concentration of 0.3 g/L, and a reaction time of 60 min. The kinetics data were fitted with first-order (Equation (1)), second-order (Equation (2)), and third-order reaction kinetics equations (Equation (3)) to investigate the characteristics of this heterogeneous Fenton-like reaction for the removal of COD from Maotai-flavored Baijiu wastewater [38–40].

$$\ln \frac{C_0}{C_T} = K_1 t \quad (1)$$

$$C_t^{-1} - C_0^{-1} = K_1 t \quad (2)$$

$$\frac{1}{2}\left(C_t^{-2} - C_0^{-2}\right) = K_1 t \quad (3)$$

In the above equations, "$K_1$" represents the degradation rate constant of an aqueous solution of Maotai-flavored Baijiu wastewater in units of $min^{-1}$. "$C_t$" denotes the concentration of the solution at time t in mg/L, while "$C_0$" signifies the initial concentration of the solution in mg/L, with "t" representing the reaction time in minutes.

In Figure 10, the heterogeneous Fenton-like reaction shows the highest fit to the third-order reaction kinetics equation, with a coefficient of determination of 0.99184. This coefficient of determination is significantly higher than those of the first-order and second-order equations. Therefore, the heterogeneous Fenton-like oxidation reaction involving the homemade Mn-Fe (2:1 wt%) catalyst is best modeled by third-order reaction kinetics:

$$\frac{1}{2}\left(Ct^{-2} - C^{-2}\right) = \left(5.56145 \times 10^{-5}\right)x + 4.06675 \times 10^{-4} \quad (4)$$

In the literature, it has been proposed that the main oxides present in the Fenton reaction are hydroxyl radicals (·OH) and superoxide anion radicals($\cdot O^{2-}$) [7]. The oxidation of complex organic matter by hydroxyl radicals, which depends on the generation of hydroxyl radicals to stimulate a series of radical reactions, is typically conducted through the following pathway [1,7,35,36]:

Polyols and sugars such as starch and sucrose undergo dehydrogenation by hydroxyl radical reactions, where C-C bonds are broken and oxidized to $CO_2$.

Water-soluble macromolecules, along with vinyl compounds, undergo hydroxyl radical reactions with C=C breakage, resulting in the production of $CO_2$.

As hydroxyl radicals can only oxidize saturated aliphatic and saturated aliphatic carbonyl compounds to carboxylic acids, the contribution of these radicals to the removal rate of COD is low.

Aromatic rings in aromatic compounds are broken down by the action of hydroxyl radicals to form aliphatic compounds, thereby enhancing their biodegradability.

·OH decomposes chromogenic radicals in dyes, facilitating decolorization and COD removal.

The effluent of the heterogeneous Fenton-like reaction was analyzed using GC–MS with solid-phase microextraction to detect small molecules with melting and boiling points below 300 °C.

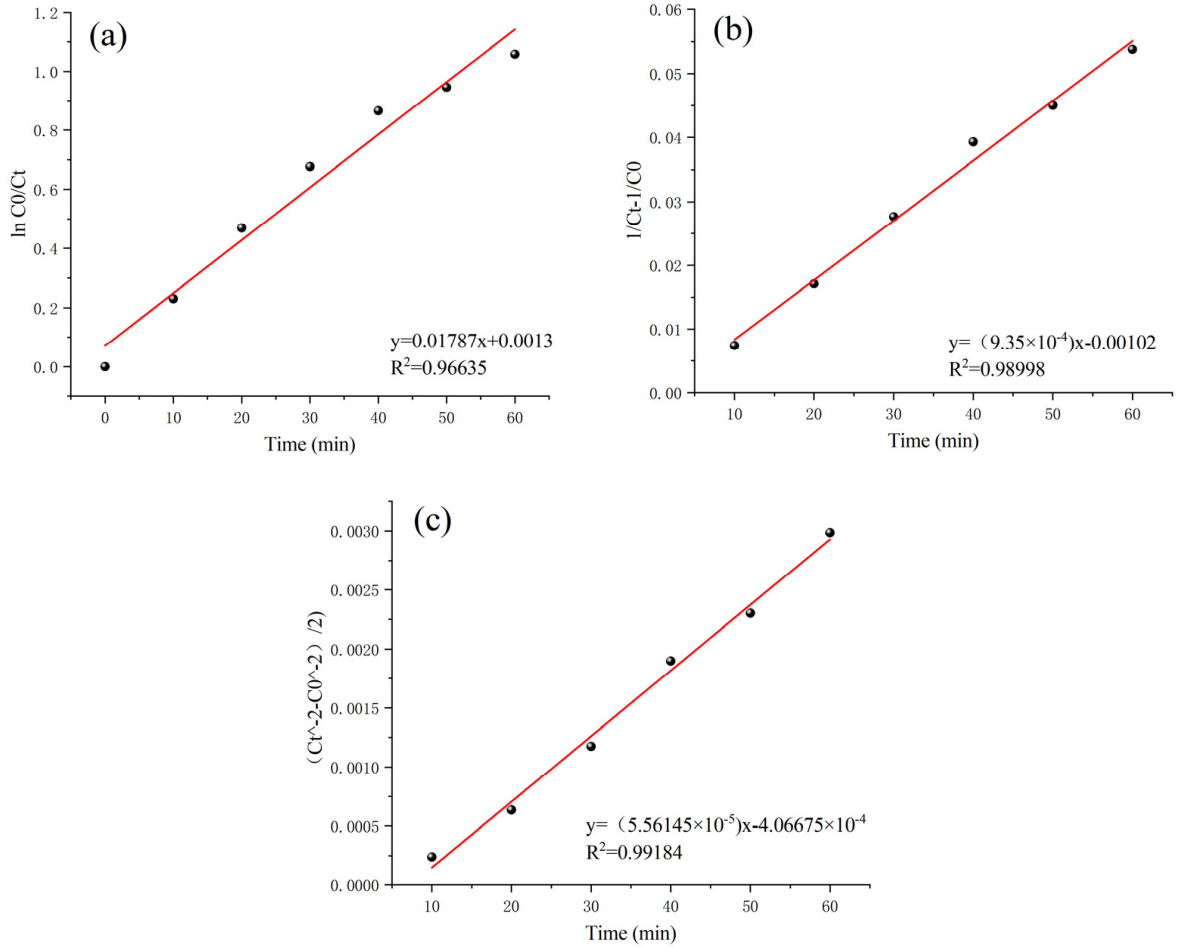



**Figure 10.** Linear fit regression results for response order: (**a**) first-order response; (**b**) second-order response; (**c**) third-order response.

Comparison of the test results with the hydroxyl radical oxidation theory revealed that the heterogeneous Fenton-like reaction was consistent with this theory (Table 3). The reaction effectively treated sugars, water-soluble macromolecules, and aromatics in the wastewater; however, the presence of aliphatic compounds after the reaction indicated that the heterogeneous Fenton-like reaction was less effective in treating aliphatic and saturated aliphatic carbonyl compounds.

**Table 3.** Analysis of GC–MS detection results.

| Organic Substance | Match Score | Percentage (%) | Estimated Concentration (mg/L) | Molecular Formula | C | H | O | Cl | S | N | P | I | Si | Br | Molecular Mass | COD Conversion Factor |
|---|---|---|---|---|---|---|---|---|---|---|---|---|---|---|---|---|
| Oxime-methoxyphenyl | 82.8 | 0.88 | 0.130358919 | $C_8H_9NO_2$ | 8 | 9 | 2 | | | 1 | | | | | 151.2 | 1.957671958 |
| Cycloheptasiloxane, tetramethyl | 91.7 | 1.53 | 0.342745045 | $C_{14}H_{42}O_7Si_7$ | 14 | 42 | 7 | | | | | | 7 | | 519.1 | 1.294548257 |
| o-Hydroxybiphenyl | 96.7 | 5.12 | 0.564091429 | $C_{12}H_{10}O$ | 12 | 10 | 1 | | | | | | | | 170.2 | 2.632197415 |
| Hexadecamethylcyclooctasiloxane | 96.6 | 0.52 | 0.116477292 | $C_{16}H_{48}O_8Si_8$ | 16 | 48 | 8 | | | | | | 8 | | 593.2 | 1.29467296 |
| 1,2,4-Triazine-3,5(2H.) | 51.2 | 0.98 | 0.365261591 | $C_3H_3N_3O_2$ | 3 | 3 | 2 | | | 2 | | | | | 113.1 | 0.778072502 |
| 2-([1,1′-Biphenyl]-2-yloxy) | 93.8 | 44.15 | 5.196572064 | $C_{14}H_{14}O_2$ | 14 | 14 | 2 | | | | | | | | 214.3 | 2.463835744 |
| 3-Methyl-1-(trimethylsiloxy) | 50.2 | 0.94 | 0.108335 | $C_{10}H_{20}OSi$ | 10 | 20 | 1 | | | | | | 1 | | 184.4 | 2.51626898 |
| 2-(3-Iodopropyl)-1,3-dioxolane | 50.5 | 1.01 | 0.285931815 | $C_6H_{11}IO_2$ | 6 | 11 | 2 | | | | | 1 | | | 242.1 | 1.024370095 |
| N-(Methoxymethyl)-1,1-diphenyl-N-[(trimethylsilyl)methyl]methylamine | 62.3 | 1.15 | 0.129396349 | $C_{19}H_{27}NOSi$ | 19 | 27 | 1 | | | 1 | | | 1 | | 313.5 | 2.577352472 |
| o-chlorobromobenzene | 50.6 | 1.12 | 0.353404545 | $C_4H_6BrC_1$ | 4 | 6 | | 1 | | | | | | 1 | 191.5 | 0.919060052 |
| 1-Acenaphthenol | 60.4 | 35.01 | 3.857195491 | $C_{12}H_{10}O$ | 12 | 10 | 1 | | | | | | | | 170.2 | 2.632197415 |
| Triphenylphosphine oxide | 95.9 | 0.85 | 0.10088375 | $C_{18}H_{15}OP$ | 18 | 15 | 1 | | | | 1 | | | | 278.3 | 2.443406396 |
| 3,5-Dimethylphenyl terephthalate | 51.1 | 1.47 | 0.193849527 | $C_{18}H_{18}O_4$ | 18 | 18 | 4 | | | | | | | | 298.3 | 2.199128394 |
| Ethyl 1,3-dithiane-2-carboxylate | 62.5 | 0.76 | 0.147162917 | $C_7H_{12}O_2S_2$ | 7 | 12 | 2 | | 2 | | | | | | 192.3 | 1.497659906 |
| look for a draw (chess) | | 95.49 | 11.89166573 | | | | | | | | | | | | | |

Although the results of this heterogeneous Fenton-like reaction are compatible with the theory of hydroxyl radical oxidation, numerous studies [33–36,41] have shown that the free radicals in the reaction exist for a short period due to their poor stability. Thus, further exploration is needed to determine whether hydroxyl radicals play a dominant role in the reaction. To investigate the catalytic mechanism of the reaction, the catalytic mechanism of this heterogeneous Fenton-like process was examined using tertiary butyl alcohol (TBA) as a quencher of the oxidative activity (Equation (5)) of ·OH and para-benzoquinone (BQ) as a quencher of $\cdot O^{2-}$ (Equation (6)) [42,43].

$$\cdot OH + C_4H_{10}O \rightarrow \cdot C_4H_9O + H_2O \quad (5)$$

$$\cdot O^{2-} + C_6H_6O_2 \rightarrow \cdot C_6H_5O_2 + O_2 \quad (6)$$

The formula for the quenching rate of ·OH was as follows [30,31]:

$$\cdot OH \text{ quenching rate } (\%) = [1 - \text{Kapp (quenching)}/\text{Kapp (base)}] \times 100\% \quad (7)$$

The quenching data were fitted to the third-order kinetic model of the heterogeneous Fenton-like reaction (Table 4), and a ·OH quenching rate of 75% was obtained.

**Table 4.** Kinetic fits for tert-butanol reactions.

| Dynamics (Math.) | Kinetic Model | $R^2$ | K Value/$min^{-1}$ |
|---|---|---|---|
| First order | $y = -0.0008x + 0.0113$ | 0.9837 | 0.0008 |
| Second order | $y = -2 \times 10^{-5}x + 0.0003$ | 0.9705 | 0.00002 |
| Third order | $y = 8 \times 10^{-5}x + 0.0004$ | 0.9935 | 0.00008 |

The experiments were conducted under the optimal reaction parameters with 10 mmol/L TBA and 10 mmol/L BQ. According to the results shown in Figure 11, the COD degradation rate was 66% without the addition of a quenching agent, 59 ± 3% with the addition of BQ, 32 ± 3% with the addition of TBA, and 25 ± 3% with the addition of both.

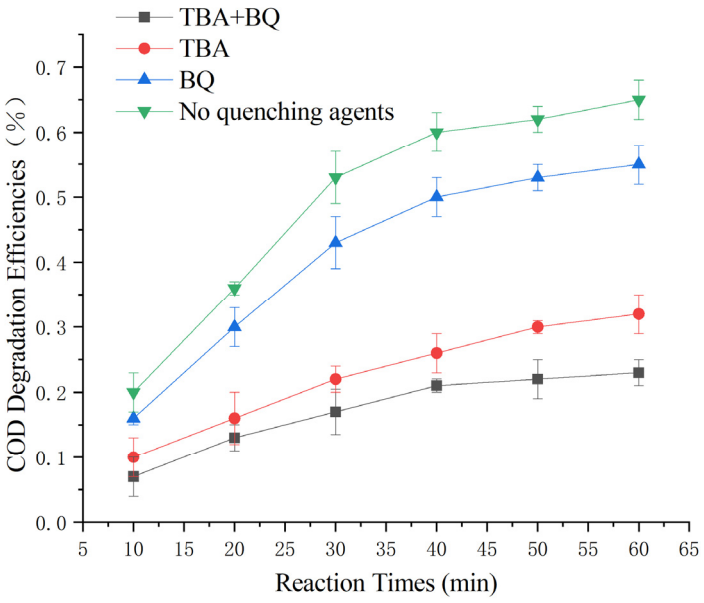



**Figure 11.** Study of COD degradation rate by different radicals.

The results revealed that ·OH plays a dominant role in this heterogeneous Fenton-like reaction, while $\cdot O^{2-}$ plays an auxiliary oxidation role. Additionally, the catalyst was found to have a certain adsorption effect on pollutants in the experiment.

On the basis of the XPS and GC–MS results as well as the results of the free radical capture experiments, the mechanism of the heterogeneous Fenton-like reaction involving this catalyst is presumed to be as follows (The process is illustrated in Figure 12): first, pollutants are adsorbed onto the surface of the catalyst; second, $Fe^{3+}$ precipitated on the active sites on the surface of the catalyst reacts with $Mn^{2+}$ in the following two pathways [28]: First, $Fe^{3+}$ and $Mn^{2+}$ react with hydrogen peroxide to produce superoxide radicals, hydroxyl radicals, and superoxide anion radicals.

$$Fe^{3+} + H_2O_2 \rightarrow Fe^{2+} + \cdot OOH + H^+ \quad (8)$$

$$Mn^{2+} + H_2O_2 \rightarrow Mn^{3+} + \cdot O^{2-} + \cdot OH \quad (9)$$

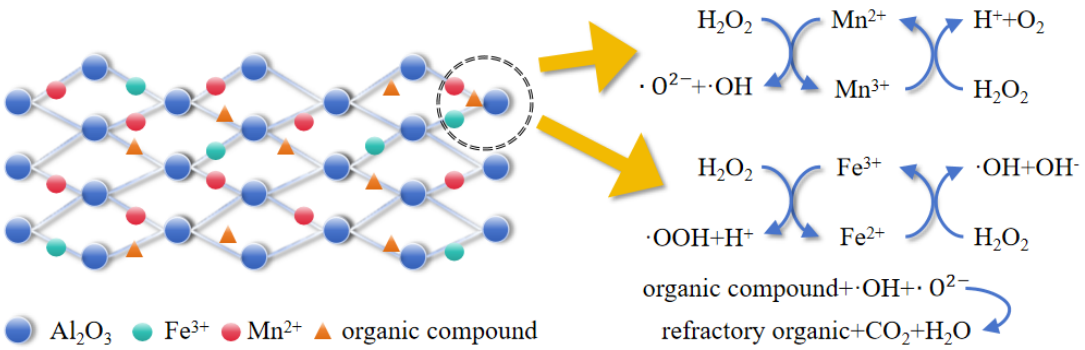



**Figure 12.** Mn-Fe/Al reaction mechanism diagram.

The $Fe^{2+}$ generated from the above reaction reacts with $Mn^{3+}$. $Fe^{2+}$ continues to react with hydrogen peroxide to generate the hydroxyl radicals needed for this heterogeneous Fenton-like process.

$$Fe^{2+} + H_2O_2 \rightarrow Fe^{3+} + \cdot OH + OH^- \quad (10)$$

$$Mn^{3+} + H_2O_2 \rightarrow Mn^{2+} + H^+ + O_2 \quad (11)$$

Manganese and iron mix with each other to form manganese–iron dual active centers in the system, which accelerate the electron transfer process through charge rearrangement. Additionally, this dual-active center structure exhibits stronger catalytic synergy than a single-active component structure. The $Mn^{2+}$ and $Mn^{3+}$ generated by the reaction accelerate the cycling of $Fe^{2+}/Fe^{3+}$.

$$\cdot OOH \rightarrow H^+ + \cdot OH + OH^- \quad (12)$$

$$Mn^{2+} + Fe^{3+} \rightarrow Mn^{3+} + Fe^{2+} \quad (13)$$

The generated ·OH and $\cdot O^{2-}$ radicals oxidize the organic matter adsorbed on the surface of the catalyst and decompose it to produce $CO_2$, $H_2O$, small-molecule inorganic acids and other products, reducing the COD in the wastewater.

## 3. Materials and Methods

### *3.1. Materials and Reagents*

γ-$Al_2O_3$ was used in the form of a 2~4 mm spherical solid; ferric nitrate hydrate ($Fe(NO_3)_3 \cdot 9H_2O$), manganese nitrate ($Mn(NO_3)_2$), and copper nitrate trihydrate ($Cu(NO_3)_2$-$3H_2O$) were obtained from Shanghai McLean Biochemical Technology (Shanghai, China). All chemicals were of analytical grade (AR) and did not need additional purification.

### *3.2. Synthesis of Catalysts*

The preparation method is outlined in Figure 13. γ-$Al_2O_3$ was used as the carrier, and $Mn(NO_3)_2$, $Fe(NO_3)_3 \cdot 9H_2O$, and $Cu(NO_3)_2 \cdot 3H_2O$ were used as the raw materials. The process involved washing 2~4 mm γ-$Al_2O_3$ with ultrapure water until the filtrate was

clear, followed by calcination at 600 °C for 4 h in a muffle furnace with subsequent static cooling [23]. After cooling, 100 g of γ-$Al_2O_3$ was weighed into a beaker, soaked in ultrapure water for 12 h, and filtered, and the amount of absorbed water was calculated.

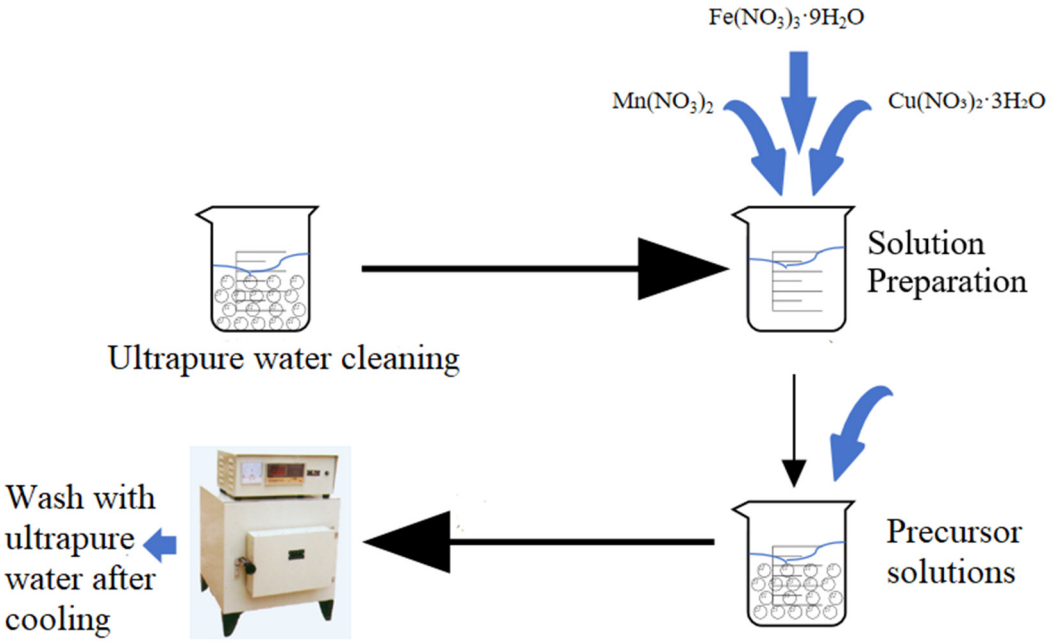



**Figure 13.** Preparation process of γ-$Al_2O_3$ (Mn, Fe, Cu).

The precursors $Mn(NO_3)_2$, $Fe(NO_3)_3·9H_2O$, and $Cu(NO_3)_2·3H_2O$ were loaded onto γ-$Al_2O_3$ using the equal volume impregnation method. The precursor solution was thoroughly mixed in a beaker, and γ-$Al_2O_3$ was placed in another beaker. The mixed solution was poured into the beaker containing γ-$Al_2O_3$ under continuous stirring. The reaction proceeded at room temperature for 12 h with constant stirring to ensure uniform impregnation. Subsequently, the impregnated material was dried in a constant temperature drying oven at 80 °C, followed by calcination at 600 °C for 4 h in a muffle furnace. After cooling, the material was cleaned with ultrapure water, dried, and stored for further use.

By controlling the addition amount of precursor solution and adjusting the type and content of active ingredients in the catalyst, 14 catalysts with different ratios were prepared, as detailed in Table 5. The experimental results (Section 2.2) indicated that the catalysts Mn-Fe (2:1 wt%) and Mn-Fe (2:2 wt%) exhibited the most effective catalytic performance, taking into account considerations such as cost effectiveness and catalyst stability [30–32]. Consequently, only these two catalysts were utilized for catalyst characterization.

**Table 5.** Novel catalysts with different active components.

| Active Ingredients | Proportional |
|---|---|
| Mn-Fe | 1:1 wt%; 2:1 wt%; 3:1 wt%; 2:2 wt%; 3:3 wt% |
| Mn-Cu | 1:1 wt%; 2:1 wt%; 3:1 wt%; 2:2 wt%; 3:3 wt% |
| Mn-Fe-Cu | 1:1:1 wt%; 2:2:1 wt%; 3:2:1 wt% |

### *3.3. Characterization of the Catalysts*

A Brunauer–Emmett–Teller (BET) automatic surface area and porosity analyzer (Mac, ASAP2460, Micromeritics, Norcross, GA, USA) was used for BET microstructural analysis, and $N_2$ adsorption was used to determine the surface area and pore structure of the materials. The elemental composition and valence states of the samples were analyzed using X-ray photoelectron spectroscopy (XPS) on a Thermo K–alpha spectrometer (Norristown, PA, USA) with monochromated Al Kα radiation and a dual X-ray source. The baseline

calibration data were obtained using $C_{1s}$ (284.60 eV). X-ray diffraction analysis (XRD) was conducted using a Bruker D8 ADVANCE instrument (Billerica, MA, USA). Additionally, scanning electron microscopy(SEM; Gemini 300, Zeiss, Oberkochen, Germany) was utilized to characterize the morphology and microstructure of the samples.

### *3.4. Heterogeneous Fenton-like Experiment*

Water samples (200 mL) were adjusted to the required pH before being poured into a 500 mL cylinder with an aeration device at the bottom for continuous aeration and stirring during the reaction. The water samples had a COD concentration of 35 ± 3 mg/L. An appropriate amount of $H_2O_2$ solution was added, followed by the introduction of a specific quantity of catalyst to initiate the reaction. The entire reaction took place at room temperature, following the parameters described in Section 2.

Immediately after the designated time elapsed, 50 mL of supernatant was extracted and centrifuged at 2000 r/min. The sample underwent wet digestion, and COD was measured using the potassium dichromate method [44–46]. To analyze the variations in organic pollutants in the water samples before and after the reaction, a gas chromatography–mass spectrometry (GC–MS) instrument (Agilent, 7890A GC-5975C MS, Santa Clara, CA, USA) was used to characterize the composition of the water samples.

## 4. Conclusions

A simple impregnation method for constructing heterogeneous Fenton-like catalysts is herein proposed. The results demonstrated that this catalyst could effectively remove COD from Maotai-flavored Baijiu wastewater and exhibited good stability for reuse. The reaction primarily depended on oxidation by hydroxyl radicals and was consistent with a third-order kinetic equation. The active components, Mn and Fe, loaded on the catalyst surface significantly enhanced the effectiveness of the heterogeneous Fenton-like reaction. They formed a synergistic catalytic dual-active center structure. These findings are highly significant for the practical application of heterogeneous Fenton-like technology, highlighting its potential in the development of advanced oxidation processes based on heterogeneous Fenton-like systems. This study represents an initial investigation of this reaction. Further optimization experiments are necessary for practical applications, such as reducing the catalyst dosage, indicating that there is some distance to go before practical implementation. Following the completion of the study, bio-toxicity testing was not conducted on the water samples.

**Author Contributions:** Conceptualization, B.L. and J.L.; methodology, B.L. and Q.K.; software, Y.Y.; validation, F.G. and B.L.; formal analysis, Y.Y. and H.H.; investigation, Y.Y. and Q.K.; resources, B.L. and J.L.; data curation, X.Y. and Y.Y.; writing—original draft preparation, Y.Y.; writing—review and editing, Y.Y. and F.G.; visualization, H.N. and Y.L.; supervision, X.Z. (Xuanyu Zhou) and S.W.; project administration, W.H. and J.L.; funding acquisition, J.L. and X.Z. (Xiang Zhou). All authors have read and agreed to the published version of the manuscript.

**Funding:** This research was funded by Study on the application of advanced oxidation technology for deep treatment of wastewater in Maotai-flavor Baijiu industrial, grant number 222357.

**Data Availability Statement:** The raw data supporting the conclusions of this article will be made available by the authors on request.

**Acknowledgments:** This study was supported by the funding and technical assistance from China Municipal Engineering Zhongnan Design and Research Institute. We thank them for their support throughout our research process. We also acknowledge Natural Science Foundation of Sichuan Province (No. 2022NSFSC0221) for partially supporting this study.

**Conflicts of Interest:** Authors Jinyin Li and Weiwei Huang were employed by the company China Municipal Engineering Zhongnan Design and Research Institute Co., Ltd. Author Xiang Zhou was employed by the company Suyi Design Group Co., Ltd. The remaining authors declare that the research was conducted in the absence of any commercial or financial relationships that could be construed as a potential conflict of interest.

## References


1. Latessa, S.H.; Hanley, L.; Tao, W. Characteristics and Practical Treatment Technologies of Winery Wastewater: A Review for Wastewater Management at Small Wineries. *J. Environ. Manag.* **2023**, *342*, 118343. [CrossRef]
2. Li, Y.Y.; Liu, X.Q.; Zhang, L.; Yuan, H.; Liu, C. The Law of the Residual COD in Distilled Spirit Wastewater after Two Stages of Biochemical Treatment. *Appl. Mech. Mater.* **2014**, *675–677*, 596–601. [CrossRef]
3. Liu, C.; Liu, X.Q.; Xiong, C.; Cai, Z.L.; Xiang, K. Comparative Study on the Anaerobically Methanogenic Results of Sauce Sweet Model Liquor and Fen-Flavor Liquor Wastewater. *Adv. Mater. Res.* **2013**, *726–731*, 2636–2640. [CrossRef]
4. Fu, J.X.; Li, H.M.; Yu, P.F.; Zhao, K. Research on Waste Materials with Decentralized White Spirit Wastewater Pretreatment by Fe-C Micro-Electrolysis. In Proceedings of the International Conference on Machine Tool Technology and Mechatronics Engineering, Guilin, China, 22–23 June 2014.
5. Moletta, R. Winery and Distillery Wastewater Treatment by Anaerobic Digestion. *Water Sci. Technol.* **2005**, *51*, 137–144. [CrossRef] [PubMed]
6. Babuponnusami, A.; Sinha, S.; Ashokan, H.; Paul, M.V.; Hariharan, S.P.; Arun, J.; Gopinath, K.; Le, Q.H.; Pugazhendhi, A. Advanced Oxidation Process (AOP) Combined Biological Process for Wastewater Treatment: A Review on Advancements, Feasibility and Practicability of Combined Techniques. *Environ. Res.* **2023**, *237*, 116944. [CrossRef] [PubMed]
7. Machado, F.; Teixeira, A.; Ruotolo, L. Critical Review of Fenton and Photo-Fenton Wastewater Treatment Processes over the Last Two Decades. *Int. J. Environ. Sci. Technol.* **2023**, *20*, 13995–14032. [CrossRef]
8. Bielski, B.H.J.; Cabelli, D.E.; Arudi, R.L.; Ross, A.B. Reactivity of HO2/O2 Radicals in Aqueous Solution. *J. Phys. Chem. Ref. Data* **1985**, *14*, 1041–1100. [CrossRef]
9. Wang, X.; Wang, P.; Ma, J.; Liu, H.; Ning, P. Synthesis, Characterization, and Reactivity of Cellulose Modified Nano Zero-Valent Iron for Dye Discoloration. *Appl. Surf. Sci.* **2015**, *345*, 57–66. [CrossRef]
10. Wang, J.; Chang, F.; Zheng, M. Advanced Treatment of Coking Wastewater by Polyaluminum Silicate Sulfate for Organic Compounds Removal. *Int. J. Environ. Res. Public Health* **2023**, *20*, 6342. [CrossRef]
11. Qian, W.; Huang, H.; Diao, Z.; Li, H.; Liu, H.; Ye, M.; Deng, Y.; Xu, Z. Advanced Treatment of Dye Wastewater Using a Novel Integrative Fenton-like/MnO2-Filled Upward Flow Biological Filter Bed System Equipped with Modified Ceramsite. *Environ. Res.* **2021**, *194*, 110641. [CrossRef]
12. Wan, Z.; Wang, J. Fenton Oxidation of Municipal Secondary Effluent: Comparison of Fe/Ce-RGO (Reduced Graphene Oxide) and Fe2+ as Catalysts. *Environ. Sci. Pollut Res.* **2018**, *25*, 31358–31367. [CrossRef] [PubMed]
13. Huang, T.; Zhang, G.; Zhang, N.; Ye, J.; Lu, P. $Fe^0$-$H_2O_2$ for Advanced Treatment of Citric Acid Wastewater: Detailed Study of Catalyst after Several Times Use. *Chem. Eng. J.* **2018**, *336*, 233–240. [CrossRef]
14. Zhu, J.; Zhu, M.; Peng, J. Fenton-like Degradation of Bisphenol A by $Fe_3O_4$ Rhombic Dodecahedrons. *New J. Chem.* **2023**, *47*, 10857–10865. [CrossRef]
15. Tolba, A.; Alalm, M.G.; Elsamadony, M.; Mostafa, A.; Afify, H.; Dionysiou, D.D. Modeling and Optimization of Heterogeneous Fenton-like and Photo-Fenton Processes Using Reusable $Fe_3O_4$-MWCNTs. *Process Saf. Environ. Prot.* **2019**, *128*, 273–283. [CrossRef]
16. Guo, M.; Lu, M.; Zhao, H.; Lin, F.; He, F.; Zhang, J.; Wang, S.; Dong, P.; Zhao, C. Efficient Electro-Fenton Catalysis by Self-Supported CFP@$CoFe_2O_4$ Electrode. *J. Hazard. Mater.* **2022**, *423*, 127033. [CrossRef] [PubMed]
17. Feng, J.; Zhang, Y. Ascorbic Acid Enhanced $CuFe_2O_4$-Catalyzed Heterogeneous Photo-Fenton-like Degradation of Phenol. *J. Environ. Chem. Eng.* **2023**, *11*, 111009. [CrossRef]
18. Leichtweis, J.; Carissimi, E.; Hagemann, U.; Ulbricht, M.; Fischer, L. $NiFe_2O_4$/Biochar Decorated Porous Polymer Membranes for the Flow-through Photo-Fenton Degradation of Tetracycline. *Chem. Eng. J.* **2023**, *477*, 147203. [CrossRef]
19. Cheng, Z.; Luo, S.; Li, X.; Zhang, S.; Nguyen, T.T.; Guo, M.; Gao, X. Ultrasound-Assisted Heterogeneous Fenton-like Process for Methylene Blue Removal Using Magnetic $MnFe_2O_4$/Biochar Nanocomposite. *Appl. Surf. Sci.* **2021**, *566*, 150654. [CrossRef]
20. Bautista, P.; Mohedano, A.F.; Menendez, N. Catalytic Wet Peroxide Oxidation of Cosmetic Wastewaters with Fe-Bearing Catalysts. *Catal. Today* **2010**, *151*, 148–152. [CrossRef]
21. Liu, P.; He, S.; Wei, H.; Wang, J.; Sun, C. Chenglin Characterizationof $\alpha$-$Fe_2O_3$/$\gamma$-$Al_2O_3$ Catalysts for CatalyticWet Peroxide Oxidation of m-Cresol. *Ind. Eng. Chem. Res.* **2015**, *54*, 130–136. [CrossRef]
22. Lim, H.; Lee, J.; Jin, S.; Kim, J.; Yoon, J.; Hyeon, T. Highly Active Heterogeneous Fenton Catalyst Using Iron Oxide Nanoparticles Immobilized in Alumina Coated Mesoporous Silica. *Chem. Commun.* **2006**, *4*, 463–465. [CrossRef] [PubMed]
23. Prins, R. On the Structure of $\gamma$-$Al_2O_3$. *J. Catal.* **2020**, *392*, 336–346. [CrossRef]
24. Wang, J.; Liu, C.; Yin, J.; Luo, J. Characteristic Reflection Peak and Its Origin of Nanostructured Material Containing Small Metal Nanoparticles: Two Case Studies. *Plasmonics* **2023**, *9*, 551–559. [CrossRef]
25. Liu, J. Characterizing Industrial Catalysts: Challenges and Opportunities. *Microsc. Microanal.* **2001**, *7*, 1098–1099. [CrossRef]
26. Martins, A.R.; Carvalho, L.S.; Reyes, P.; Grau, J.M.; Rangel, M.D.C. Hydrogen Production on Alumina-Supported Platinum Catalysts. *Mol. Catal.* **2016**, *429*, 1–9. [CrossRef]
27. Liang, X.; Li, Y.; Wei, G.; He, H.; Stucki, J.W.; Ma, L.; Pentrakova, L.; Pentrák, M.; Zhu, J. Heterogeneous Reduction of 2-Chloronitrobenzene by Co-Substituted Magnetite Coupled with Aqueous $Fe^{2+}$: Performance, Factors, and Mechanism. *ACS Earth Space Chem.* **2019**, *3*, 728–737. [CrossRef]

28. Li, Y.; Wei, G.; Liang, X.; Zhang, C.; Arai, Y. Metal Substitution-Induced Reducing Capacity of Magnetite Coupled with Aqueous Fe(II). *ACS Earth Space Chem.* **2020**, *4*, 905–911. [CrossRef]
29. Wang, Y.; Zhao, G.; Chai, S.; Zhao, H.; Wang, Y. Three-Dimensional Homogeneous Ferrite-Carbon Aerogel: One Pot Fabrication and Enhanced Electro-Fenton Reactivity. *ACS Appl. Mater. Interfaces* **2013**, *5*, 842–852. [CrossRef] [PubMed]
30. Ling, Y.; Long, M.; Hu, P.; Chen, Y.; Huang, J. Magnetically Separable Core-Shell Structural γ-$Fe_2O_3$@Cu/Al-MCM-41 Nanocomposite and Its Performance in Heterogeneous Fenton Catalysis. *J. Hazard. Mater.* **2014**, *264*, 195–202. [CrossRef]
31. Wang, Y.; Zhu, L.; Yang, X.; Shao, E.; Deng, X.; Liu, N.; Wu, M. Facile Synthesis of Three-Dimensional $Mn_3O_4$ Hierarchical Microstructures and Their Application in the Degradation of Methylene Blue. *J. Mater. Chem. A* **2015**, *3*, 2934–2941. [CrossRef]
32. Yu, L.; Zhang, G.; Liu, C.; Lan, H.; Liu, H.; Qu, J. Interface Stabilization of Undercoordinated Iron Centers on Manganese Oxides for Nature-Inspired Peroxide Activation. *ACS Catal.* **2018**, *8*, 1090–1096. [CrossRef]
33. Gu, L.; Nie, J.-Y.; Zhu, N.; Wang, L.; Yuan, H.-P.; Shou, Z. Enhanced Fenton's Degradation of Real Naphthalene Dye Intermediate Wastewater Containing 6-Nitro-1-Diazo-2-Naphthol-4-Sulfonic Acid: A Pilot Scale Study. *Chem. Eng. J.* **2012**, *189–190*, 108–116. [CrossRef]
34. Masomboon, N.; Ratanatamskul, C.; Lu, M.-C. Kinetics of 2,6-Dimethylaniline Oxidation by Various Fenton Processes. *J. Hazard. Mater.* **2011**, *192*, 347–353. [CrossRef] [PubMed]
35. Carlsson, C.; Fegeant, B.; Svensson, E.; Wiklund, L.; Jonsson, M. On the Selectivity of Radical Scavengers Used To Probe Hydroxyl Radical Formation in Heterogeneous Systems. *J. Phys. Chem. C Nanomater. Interfaces* **2022**, *126*, 12435–12440. [CrossRef]
36. Lu, Q.; Liu, Y.; Li, B.; Feng, L.; Du, Z.; Zhang, L. Reaction Kinetics of Dissolved Black Carbon with Hydroxyl Radical, Sulfate Radical and Reactive Chlorine Radicals. *Sci. Total Environ.* **2022**, *828*, 153984. [CrossRef] [PubMed]
37. Guo, X.; Wang, K.; Xu, Y. Tartaric Acid Enhanced $CuFe_2O_4$-Catalyzed Heterogeneous Photo-Fenton-like Degradation of Methylene Blue. *Mater. Sci. Eng. B* **2019**, *245*, 75–84. [CrossRef]
38. Huanyan, X.U.; Wang, Y.; Shi, T.N.; Zhao, H.; Tan, Q.; Zhao, B.C.; Xiulan, H.E.; Shuyan, Q.I. Heterogeneous Fenton-like Discoloration of Methyl Orange Using $Fe_3O_4$/MWCNTs as Catalyst: Kinetics and Fenton-like Mechanism. *Front. Mater. Sci.* **2018**, *12*, 34–44.
39. Chengjie, Z.; Kaifeng, Y.; Shiyu, H.; Feng, C. Adsorption-Depended Fenton-like Reaction Kinetics in $CeO_2$-$H_2O_2$ System for Salicylic Acid Degradation. *Colloids Amp. Surf. A Physicochem. Amp. Eng. Asp.* **2018**, *553*, 456–463.
40. Audino, F.; Conte, L.O.; Schenone, A.V.; Pérez-Moya, M.; Graells, M.; Alfano, O.M. A Kinetic Study for the Fenton and Photo-Fenton Paracetamol Degradation in an Annular Photoreactor. *Environ. Sci. Pollut. Res.* **2019**, *26*, 4312–4323. [CrossRef]
41. Xi, Z.; Jin, B.X.; Shan, Z. Reaction Mechanisms Involving Peroxy Radical in the Low-Temperature Oxidation of Coal. *Fuel* **2021**, *300*, 120943. [CrossRef]
42. Pochon, A.; Vaughan, P.P.; Gan, D.; Vath, P.; Blough, N.V.; Falvey, D.E. Photochemical Oxidation of Water by 2-Methyl-1,4-Benzoquinone: Evidence against the Formation of Free Hydroxyl Radical. *J. Phys. Chem. A* **2002**, *106*, 2889–2894. [CrossRef]
43. Bakhoda, A.G.; Wiese, S.; Greene, C.; Figula, B.C.; Bertke, J.A.; Warren, T.H. Radical Capture at Nickel(II) Complexes: C–C, C–N, and C–O Bond Formation. *Organometallics* **2020**, *39*, 1710–1718. [CrossRef]
44. Xu, X.; Wang, J.; Li, J.; Fan, A.; Zhang, Y.; Xu, C.; Qin, H.; Mu, F.; Xu, T. Research on COD Measurement Method Based on UV-Vis Absorption Spectra of Transmissive and Reflective Detection Systems. *Front. Environ. Sci.* **2023**, *11*, 1175363. [CrossRef]
45. Ma, Y.; Tie, Z.; Zhou, M.; Wang, N.; Cao, X.; Xie, Y. Accurate Determination of Low-Level Chemical Oxygen Demand Using a Multistep Chemical Oxidation Digestion Process for Treating Drinking Water Samples. *Anal. Methods* **2016**, *8*, 3839–3846. [CrossRef]
46. Korenaga, T. The Continuous Determination of Filtered Chemical-Oxygen Demand with Potassium Dichromate by Means of Flow-Injection Analysis. *Bull. Chem. Soc. Jpn.* **1982**, *55*, 1033–1038. [CrossRef]


**Disclaimer/Publisher's Note:** The statements, opinions and data contained in all publications are solely those of the individual author(s) and contributor(s) and not of MDPI and/or the editor(s). MDPI and/or the editor(s) disclaim responsibility for any injury to people or property resulting from any ideas, methods, instructions or products referred to in the content.